Science of the Total Environment 912 (2024) 169046

Contents lists available at ScienceDirect

Science of the Total Environment

journal homepage: www.elsevier.com/locate/scitotenv

On groundwater flow and shallow geothermal potential: A surrogate model for regional scale analyses

Alberto Previati *, Giovanni Crosta

DISAT – Department of Earth and Environmental Sciences, University of Milano-Bicocca, Piazza della Scienza, 4, Milan 20126, Italy

HIGHLIGHTS

- A new approach to assess the regional geothermal potential with groundwater flow
- Numerically derived g-functions considering advection to evaluate the potential
- Numerical results implemented at regional scale by machine learning surrogate model
- Benefits of groundwater flow discussed considering the usable/unusable potential

GRAPHICAL ABSTRACT

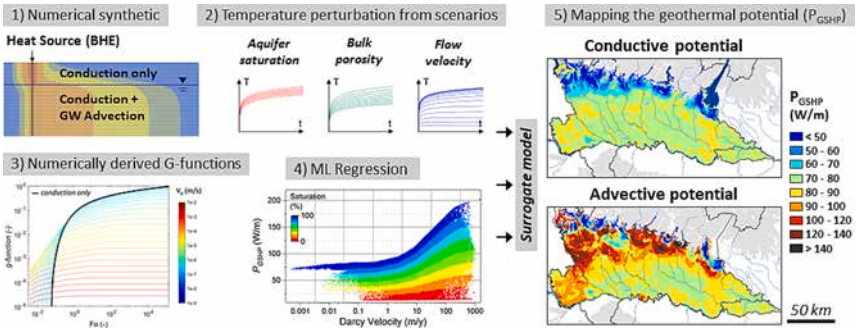

ARTICLE INFO

Editor: Christian Herrera

Keywords:
Shallow geothermal energy
Groundwater advection
Geothermal potential
Surrogate model
Machine learning regression
Regional scale

ABSTRACT

Many cities worldwide lay upon alluvial aquifers which have a great potential for low temperature geothermal installations thanks to the thermal diffusive properties of saturated porous media and the constant temperature of the subsurface. In addition, aquifers with fast moving groundwater have a higher potential due to the additional energy replenishment by advection, which is often underestimated.

This work aims at bridging the gap between quantitative hydro-thermal numerical analysis and regional scale assessment developing a process-based surrogate model for the estimation of the thermal exchange (geothermal) potential of ground source heat pumps (GSHP) considering groundwater advection. The proposed method is based on a synthetic 3D FEM model reproducing the infinite line source configuration and introducing groundwater advection. Conductive/advective g-functions were derived from the numerically simulated space-time thermal perturbation for a comprehensive set of hydrogeological regimes, and a surrogate model was developed by a machine learning (ML) regression of the thermal response of the system. This solution, beyond the run time of the numerical study and the ML training phase, is very fast, applicable at any scale and scalable to any desired depth.

The trained model can be used to predict the geothermal potential of GSHP for almost all sedimentary basins around the world upon the availability of the required input data (aquifer thickness and saturation, aquifer porosity and groundwater flow velocity). In this study, large scale geothermal potential maps were generated from input layers implemented in a GIS, for a demonstrative area in northern Italy showing highly variable groundwater flow (Darcy velocity from 10^{-3} to 10^{+3} m/y). A promising increase (up to +250 %) in the thermal exchange potential of GSHP due to the contribution of advection was highlighted discussing the benefits of

* Corresponding author.
E-mail address: a.previati1@campus.unimib.it (A. Previati).

https://doi.org/10.1016/j.scitotenv.2023.169046
Received 29 September 2023; Received in revised form 28 November 2023; Accepted 30 November 2023
Available online 3 December 2023

groundwater flow and the amount of usable potential with implications on shallow geothermal energy management and development.

Nomenclature

α	Thermal diffusivity (m^2/s)
E_G	Annual energy load on the ground (kWh)
Fo	Fourier number (−)
G	G-function
i	Hydraulic gradient (−)
K	Hydraulic conductivity (m/s)
L	Length of the borehole (m)
λ	Thermal conductivity (W/mK)
L_c	Characteristic length (m)
n	Porosity (−)
Pe	Peclet number (−)
P_{ground}	Thermal exchange potential of the ground (W/mK)
P_{GSHP}	Thermal exchange potential of the GSHP (W/m)
q	Fluid specific flux or Darcy velocity (m/s)
q_h	Specific thermal power (W/m)
Q	Thermal power on the heat pump side (W)
Q_G	Thermal power on the ground side (W)
R	Reference radius for the cylindrical solution (m)
r	Radial distance from the linear heat source (m)
R_b	Thermal resistance of the borehole heat exchanger (mK/W)
R_g	Thermal resistance of the ground (mK/W)
ρc	Volumetric heat capacity (J/m^3K)
S	Aquifer saturation (%)
τ	Thermal time constant (s)
V_d	Darcy velocity (m/s)

Abbreviations/acronyms

ASHRAE	American Society of Heating, Refrigerating and Air-Conditioning Engineers
BC	Boundary condition
BHE	Borehole heat exchanger
COP	Coefficient of performance (W/W)
EFLH	Equivalent full-length load hours (h)
GSHP	Ground source heat pumps
GWHP	Groundwater heat pumps
ICS	Infinite cylindrical source
ILS	Infinite line source
ML	Machine learning
TRT	Thermal response test

1. Introduction

Shallow geothermal systems extract or inject heat from the ground by means of a heat pump. Although some electricity is required to move the heat, they are considered a renewable energy resource (EU Directive 2009/28/EC) due to the performance achieved. Ground source heat pumps (GSHP) are widely used to exchange heat with the ground using a borehole heat exchanger (BHE). Their design answers a fundamental question: how much of the ground is necessary to obtain the required thermal power? This is usually addressed by installers to maximize efficiency and minimize installation costs by evaluating: (1) the thermal properties of the ground, (2) the thermal resistance of the BHE, (3) the characteristics of the heat pumps, and (4) the long-term heat rejection and extraction to and from the ground. Thus, ignoring the characteristics of the systems (2 and 3), the sustainable heat exchange rate between the ground and a GSHP depends essentially on the thermal response of the subsurface which is influenced by the sediment type, the porosity, the saturation and the groundwater flow regime. The last one (groundwater flow) will be covered in this work proposing a new method to estimate the shallow geothermal potential considering the effects of groundwater advection and a workflow for regional scale mapping. Although there is no single definition for the geothermal potential, this quantitative indicator based on physical laws is used to describe and compare the heat exchange efficiency between the subsurface and geothermal systems (for a review on the geothermal potential see Bayer et al., 2019).

Many methods (most of which are reviewed by Spitler and Bernier, 2016) exist to estimate the maximum sustainable thermal load of a BHE. Rules of thumb based on heat extraction rates from existing installations include those from the German (VDI 4640/2, 2001) and Swiss (SIA 384/6, 2010) guidelines. Analytical equations based on the heat conduction law have been implemented following Carslaw and Jaeger (1959) and Ingersoll et al. (1954) who first estimated the temperature perturbation around a BHE developing the Infinite Line Source (ILS) and the Cylindrical Line Source (CLS) solutions. The ASHRAE method of Kavanaugh and Rafferty (2014) and the G.POT method of Casasso and Sethi (2016) estimate the total length of a BHE as a function of the ground heat transfer properties derived from the thermal perturbation due to heat injection pulses of different durations (e.g. 4 h, 30 days and 10 years for the ASHRAE method). Other approaches, starting from the seminal work by Eskilson (1987) have implemented so called g-functions that estimate the ground heat transfer properties considering thermal interactions in multiple borehole configurations and arrays. Many commercial BHE design software packages, such as EED (BLOCON, 2015) and GLHEPRO (Spitler, 2000), are based on pre-calculated g-functions covering a large number of possible configurations for a BHE field and ground thermal properties.

These methods have been widely used to map the geothermal potential at regional scale with the aid of a GIS. Among others, some examples are: Galgaro et al. (2015) estimated the thermal exchange potential for a very large area from a set of heat transfer simulations with a design software; a novel method (G.POT) was proposed by Casasso and Sethi (2016) to derive the heat exchange rate from a comprehensive set of analytical heat transfer simulations (based on the ILS solution) and was used to map the geothermal potential in different areas (e.g., Italy: Casasso and Sethi, 2017; Slovenia: Casasso et al., 2017); Viesi et al. (2018) implemented in a GIS the regression of the heat extraction rate vs the thermal properties from tabulated values (VDI 4640/2, 2001); Previati and Crosta (2021) implemented the ASHRAE method for mapping the maximum heat exchange rate from spatially derived ground thermal resistances. All of the above mentioned empirical and analytical methods are fast and easy to implement in a GIS but relies solely on heat conduction and are valid only for homogeneous ground. They are therefore suitable in unsaturated or static groundwater regimes, neglecting a significant amount of heat taken up by the aquifer when groundwater flow is present.

The literature dealing with groundwater flow and heat transfer capacity of the subsurface highlight the advantages (reviewed by Banks, 2015) of moving water for a more efficient heat exchange. Signorelli et al. (2007) and Wagner et al. (2013) showed the effects of advective heat transport by analyzing empirical and numerical thermal response tests (TRT) according to different flow velocities. Numerical (Angelotti

et al., 2014; Choi et al., 2013; Fan et al., 2007; Fujii et al., 2005; García-Gil et al., 2015) and empirical (Wang et al., 2009) studies at the borehole scale demonstrated a significative increment of the heat extraction rate in advective-dominated hydrogeological settings, but their implementation at regional scale is almost lacking. Alcaraz et al. (2016) formulated the low temperature geothermal potential as the maximum power that can be exchanged with the ground, without exceeding a certain temperature increase at a given distance. This was done implementing the Moving Infinite Line Source (MILS) analytical method of Diao et al. (2004) and Sutton et al. (2003) to obtain maps of the shallow geothermal potential and the thermally affected zone for a 1km^2 large area. The large variability in the thermal response of the ground due to different flow regimes suggested by these studies (e.g. for Alcaraz et al., 2016, the geothermal potential can increase by one order of magnitude) motivates the need for tools to quantify the potential benefits of groundwater flow for the heat exchange of GSHP and a regional scale mapping method is essential to emphasize the potential of shallow geothermal installations.

Physically-based numerical modeling is the optimal tool for quantitative analysis in thermal hydrogeology (see Domenico and Schwartz, 1998 for a theoretical background; Hecht-Méndez et al., 2010 and Böttcher et al., 2019, or Piga and Casasso, 2017 for examples on analysis of GSHP and GWHP systems, respectively) but it is not feasible on a regional scale due to the enormous domain size/resolution required. Surrogate modeling (also known as metamodeling) techniques have proven to be a fast and robust tool to bridge the gap between modeling and decision support at large scales (Asher et al., 2015; Fienen et al., 2015, 2016). These techniques integrate the advantages of process-based numerical analysis into a statistical learning (or machine learning) algorithm to produce quantitative results in a fast and robust manner. Thus, a surrogate model can produce response maps of the process under study as long as the assumptions and inputs required by the underlying model are valid and available.

In this study, a surrogate model solution combining a FEM hydrothermal numerical analysis with machine learning regression is presented to quantify the geothermal potential of large-scale aquifers showing high variability in the groundwater flow regime. A novel methodology to evaluate the thermal exchange potential of GSHPs is presented addressing two main unresolved issues in regional scale assessments: 1) the quantification of the geothermal potential considering the effect of groundwater flow which is often neglected; 2) the evaluation of a non-homogeneous ground along the vertical dimension considering the unsaturated and unsaturated layers which are usually aggregated by single homogeneous depth-averaged values of thermal properties (e.g. as required by the ILS method). The method is presented following four main steps:

1. a synthetic transient-state 3D FEM numerical model reproducing a constant vertical linear heat source was used to derive the thermal perturbation in space and time covering a wide variability of groundwater flow velocity, porosity and saturation values;
2. the average thermal perturbation along cylindrical envelopes around the linear heat source was used to derive conductive/advective pseudo g-functions for a single GSHP;
3. the numerically derived g-functions were combined to obtain the thermal resistance of the ground to variable duration heat pulses and to calculate the sustainable heat exchange potential following the ASHRAE sizing method;
4. the calculated responses (i.e. geothermal potential) were used to train a machine learning regression algorithm that feeds a surrogate model applicable at any scale/resolution and scalable to any desired depth when required input data are available. The approach will be applied on a large demonstrative area showing a high variability of the groundwater flow regime.

2. Materials and methods

2.1. Configuration of the numerical model

A synthetic 3D FEM model was developed (Fig. 1) to reproduce the ILS/ICS geometric configuration and to simulate the thermal perturbation for a comprehensive set of hydrogeologic and thermal parameters, embracing different groundwater flow regimes. The external boundary conditions (BC) and model domain boundaries were designed to be sufficiently distant from the heat source to exclude interactions with the internal heat source in order to compare the numerical twin with the infinitely extended ILS/ICS analytical solutions. Moreover, the vertical dimension is 2000 times larger than the reference cylinder radius (R) making the solution comparable to the ILS/ICS assumptions with negligible boundary effects at the top and bottom of the model. Assuming the temperature perturbation symmetric with respect to a vertical plane aligned with the groundwater flow direction passing by the vertical linear heat source, the horizontally "infinite" domain was reduced to a "semi-infinite" domain to reduce the computational time. Fig. 1 shows the synthetic 3D FEM model mesh 2000 × 1000 × 100 m (L, W, H) in size, which contains a total of 83,220 triangular prism elements arranged in 20 equally spaced vertical layers. The horizontal mesh dimensions range from 0.005 m around the heat source to 50 m at the most distal locations. A set of 9 control semi-cylinders with a radius ranging from r = 0.05 m to 20 m was realized to record the temperature evolution in space and time around the heat source. The closest will be the reference cylinder for the ICS solutions (R = 0.05 m).

From the mathematical point of view, the problem is governed by the following two equations:

$$\mathrm{K}\cdot\nabla^2(\mathrm{h}) = \mathrm{S_S}\frac{\partial \mathrm{h}}{\partial \mathrm{t}} \tag{1}$$

where K (m/s) and S_S (1/m) are the hydraulic conductivity and the specific storage of the porous medium, and h (m) is the hydraulic head.

$$-\mathrm{q}\,\rho\mathrm{c_{fluid}}\cdot\nabla(\mathrm{T}) + \lambda_{\mathrm{bulk}}\cdot\nabla^2(\mathrm{T}) + \mathrm{s} = \rho\mathrm{c_{bulk}}\frac{\partial \mathrm{T}}{\partial \mathrm{t}} \tag{2}$$

where q (m/s) is the fluid specific flux (Darcy velocity), ρc (J/m^{3}K) the volumetric heat capacity, λ (W/mK) the thermal conductivity, T (K) the average element temperature, and s (J/s) is a heat source/sink term.

The first equation, results from the combination of the fluid mass conservation principle and the Darcy's law, whereas the second is derived combining the energy conservation principle and the Fourier's law. It is worth noting that in the second equation appears a source term which is imposed during the simulation along a vertical line ("ab" in Fig. 1).

Table 1 summarizes the boundary conditions applied to the numerical problem: upstream and downstream fluid 1st type (Dirichlet) BCs were used to control the hydraulic gradient and the saturation depth, while a heat source term (constant heat power) along the 21 nodes sharing the linear heat source was used to control the injected/extracted thermal power. No fluid and heat flux were considered through the top, bottom and lateral faces of the model. The head initial condition of each scenario was generated from a steady-state simulation as illustrated above and the temperature initial condition was set to a constant value of 15 °C. A 1st type (Dirichlet) temperature BC of 15 °C was also imposed to the upstream face to control the temperature of the fluid inflow to the model.

The numerical simulation for each proposed scenario is composed of two steps:

1. A steady-state simulation is performed by imposing only the fluid boundary conditions, without considering the thermal phenomenon. The velocity regime is obtained and does not vary with time;

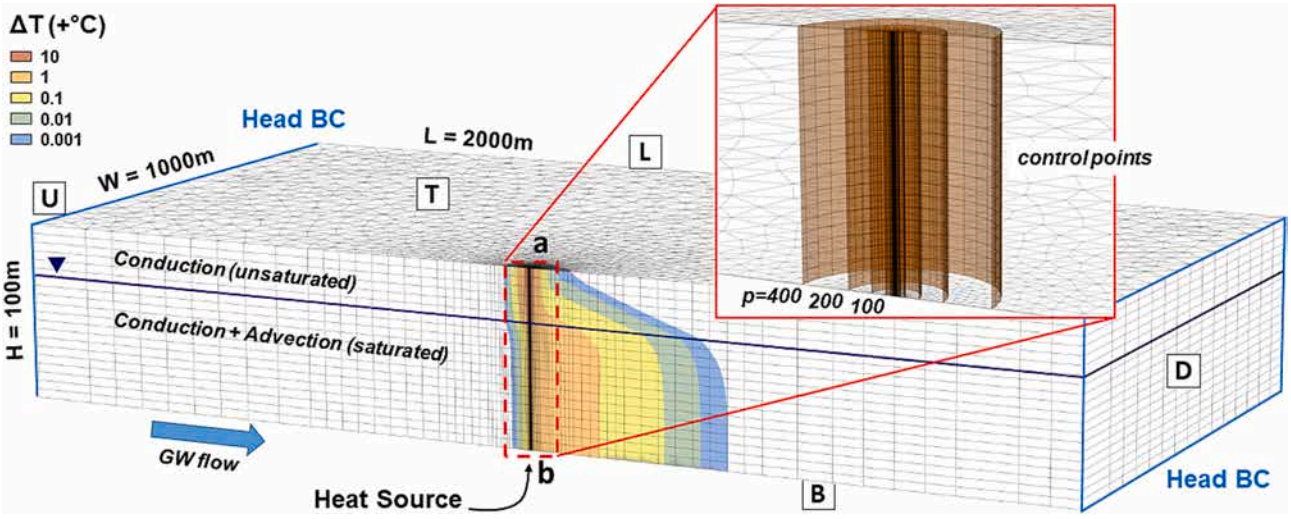

Fig. 1. Configuration of the 3D FEM numerical model for the evaluation of the radial temperature perturbation of a linear heat source ("ab"), p represents the r/R ratio (R = 0.05 m, reference radius for the ICS solution). Colored fringes show the thermal perturbation (ΔT with respect to initial conditions) after two years of simulation with a constant heat source (q) of 100 W/m. Hydrogeological parameters used in this example are: S = 70 %, n = 0.25, V_d = 5e-6 m/s (see Table 2 for their definition); for the thermal parameters refers to the text. Model boundary faces are named with letters in boxes: T = top, B = bottom, U = upstream, D = downstream, L = lateral.

Table 1
Summary of the boundary conditions (BC) and sink/source terms applied to the synthetic model. See Fig. 1 for the geometrical configuration of the described terms referring to the abbreviations in this table.

	Fluid BC	Heat BC
Upstream face (U)	Dirichlet (Ass. Head)	Dirichlet (Ass. Temp)
Downstream face (D)	Dirichlet (Ass. Head)	Neumann (No flux)
Lateral (L), top (T) and bottom (B) faces	Neumann (No flux)	Neumann (No flux)
Linear source (AB)	–	Source (Heat Power)

2. Once the velocity regime is calculated, the thermal part is activated, taking the results of the previous step as the initial condition of the fluid for a transient fluid-thermal analysis. In this stage, a linear heat source ("ab" in Fig. 1) injects constant power into the system over time. Due to the small range of temperature variations, the dependence of the fluid density on temperature is ignored.

By changing the values of the boundary conditions and parameters, several scenarios were generated to explore the variation of temperature in space and time for a comprehensive set of hydrogeological schematic settings. Each transient simulation lasted for ten years and 9 control cylinders (Fig. 1) were used to record the average temperature variation around the linear heat source with respect to the initial reference value of 15 °C. A total of 5670 transient-state simulations were performed as illustrated in Table 2.

A hydraulic gradient (i) of 1 ‰ (reasonable for many alluvial plain settings) was applied to all scenarios imposing a head difference of 2 m between the upstream and downstream fluid BCs. The Darcy velocity (V_d) was controlled by varying the isotropic hydraulic conductivity (K) according to the relationship $V_d = K{\cdot}i$. The model saturation (S) was controlled by changing the head values of the upstream BC between 1 (fully dry) and 101 m (fully saturated) and that of the downstream BC between −1 and 99 m (keeping the difference between the upstream and downstream head values at 2 m).

Table 2
Ranges of hydrogeological schematic settings investigated in this study obtained by changing the values of boundary conditions and parameters.

Parameter		Unit	Min	Max	Scenarios
V_d	Darcy velocity	m/s	1e-9	1e-2	29 (+ no flow)
n	Porosity	–	0.1	0.5	9
S	Model saturation	% of H	0	100	21

The saturated bulk thermal parameters were derived calculating the porosity-weighted arithmetic and geometric mean between the solid and the fluid phase for the volumetric heat capacity (ρc) and the thermal conductivity (λ), respectively (Woodside and Messmer, 1961):

$$\rho c_{bulk} = \rho c_{fluid} * n + \rho c_{solid} * (1 - n) \quad (3)$$

$$\lambda_{bulk} = (\lambda_{fluid})^{n} * (\lambda_{solid})^{(1-n)} \quad (4)$$

According to the German technical guidelines (VDI 4640/2, 2001), typical values of solid and fluid (water or air filling the voids) thermal parameters were assigned and combined to obtain equivalent-bulk parameters according to the scenario of porosity (Table 3). In partially saturated simulations (100 > S > 0), the bulk parameters of each layer were calculated according to the porosity and to the presence of air (unsaturated) or water (saturated).

2.2. Derivation of g-functions for groundwater flow regimes

The conductive thermal perturbation around an infinite cylindrical

Table 3
(a) Thermal parameters (λ = thermal conductivity, ρc = volumetric specific heat capacity) used in this study (from tabulated values in the German guidelines: VDI 4640/2, 2001) for the solid and fluid phase (water or air), and (b) resulting bulk parameters derived using Eqs. (3) and (4) for different values of porosity (n) and saturation.

a)			b)	Saturated		Dry	
	λ	ρc		λ_{bulk}	ρc_{bulk}	λ_{bulk}	ρc_{bulk}
	W/mK	MJ/m^{3}K	n	W/mK	MJ/m^{3}K	W/mK	MJ/m^{3}K
Solid	3.5	2	0.1	2.93	2.22	2.09	1.80
Water	0.6	4.2	0.2	2.46	2.44	1.25	1.60
Air	0.02	0.0012	0.3	2.06	2.66	0.74	1.40
			0.4	1.73	2.88	0.44	1.20
			0.5	1.45	3.10	0.26	1.00

heat source of radius R was first expressed by Carslaw and Jaeger (1959) and Ingersoll et al. (1954) with the following solution:

$$\Delta T(r,t) = \frac{q_h}{\lambda} * G(Fo,p) \tag{5}$$

where q_h is the specific heat exchange rate (W/m), λ is the thermal conductivity of the medium (W/mK) and G is the nondimensional equation (g-function) that describes the perturbation as a function of the Fourier number: $Fo = \frac{\alpha t}{R^2}$, and the radial distance (r) expressed as a multiple of the reference cylinder radius (R): $p = r/R$ (for $r > R$). A complete solution for G is given by the following integral equation proposed by Carslaw and Jaeger (1959):

$$G(Fo,p) = \frac{1}{\pi^2} \int_0^{\infty} \frac{e^{-\beta z} - 1}{J_1^2(\beta) + Y_1^2(\beta)} \left[J_0(p\beta) Y_1(\beta) - J_1(\beta) Y_0(p\beta) \right] \frac{d\beta}{\beta^2} \tag{6}$$

where $\beta = \frac{r}{2\sqrt{(t-\tau)}}$ given the thermal time constant $\tau = \frac{\rho c}{\lambda} L_c$ expressed for the characteristic length ($L_c = \frac{V}{A} = \frac{R}{2}$). The term α indicates the thermal diffusivity (m^2/s) of the ground as the ratio between the thermal conductivity (λ) and the volumetric heat capacity (ρc). The solution of G was tabulated by Ingersoll et al. (1954) for different values of Fo and p, and was implemented in Matlab® in the scope of this work.

Thus, the values of the g-function and the space-time temperature perturbation can be derived reciprocally by means of Eq. (5) for purely conductive problems. In this study, the temperature perturbation obtained by the ICS using the g-function from Eq. (6) was compared to the numerical solution described in Section 2.1 with static groundwater achieving a perfect correlation for Fourier numbers sufficiently large (small distance, large diffusivity, and large times). Fig. 2 shows a comparison between the temperature perturbation normalized by the specific power q_h (100 W/m) obtained with the two methods for $\lambda = 2$ W/mK, $\alpha = 6.6e\text{-}7$ m^2/s and different radii (r).

Similarly, the average thermal perturbation ($\overline{\Delta T}$) at a specific distance around the line source obtained from the numerical simulations described in Table 2 (i.e. the difference between the calculated temperature and the initial temperature value) was used to derive pseudo g-functions (G^*) for different groundwater flow and saturation regimes by inverting Eq. (5) into Eq. (7):

$$G^*(Fo,p) = \overline{\Delta T}(r,t) \frac{\lambda_g}{q_h} \tag{7}$$

where λ_g is the depth averaged thermal conductivity of the ground considering the saturation depth. In particular, assuming the temperature field symmetrical with respect to a vertical plane parallel to the groundwater flow direction and passing through the vertical linear heat source, the thermal perturbation at each calculation step was obtained as the average between the calculated temperature at all the nodes belonging to a specific semi-cylinder of radius r as shown in the detail of Fig. 1. Note that the configuration of the mesh nodes is also symmetrical with respect to a plane perpendicular to the groundwater flow and passing by the vertical linear heat source to achieve the same number of nodes down- and upstream with a constant angular distance. Fig. 3 shows the numerically derived conductive/advective pseudo g-functions for different values of groundwater Darcy velocity (V_d) compared to the analytical g-function (Eq. (6)) for a purely conductive solution (black line). It should be noted that the numerically derived pseudo g-functions cannot describe the full spatio-temporal temperature perturbation around the heat source since the coupled conductive/advective heat transport problem is not radial. Thus, the pseudo g-functions contain information only about the average temperature perturbation around the linear heat source which will be used later to derive the thermal resistance of the ground.

2.3. Calculation of the thermal exchange potential

Following the sizing method proposed by Kavanaugh and Rafferty (2014) in the ASHRAE handbook, the thermal response of the ground to three heat pulses of different length ($t_1 = 4$ h, $t_2 = 30$ days, $t_3 = 10$ years) was used to derive the thermal exchange potential of a single vertical BHE, considering all the hydrogeological settings summarized in Table 2. The three corresponding ground thermal resistances Rg_1, Rg_2 and Rg_3 were obtained considering the values of the numerically derived pseudo g-function (G^*) at times t_1, t_2 and t_3 (Kavanaugh and Rafferty, 2014):

$$\boldsymbol{R_{g1}} = \frac{G_1^*}{\lambda_g}; \boldsymbol{R_{g2}} = \frac{G_2^* - G_1^*}{\lambda_g}; \boldsymbol{R_{g3}} = \frac{G_3^* - G_1^*}{\lambda_g} \tag{8}$$

where λ_g is the depth averaged thermal conductivity of the ground considering the saturation depth. According to the ASHRAE method, the

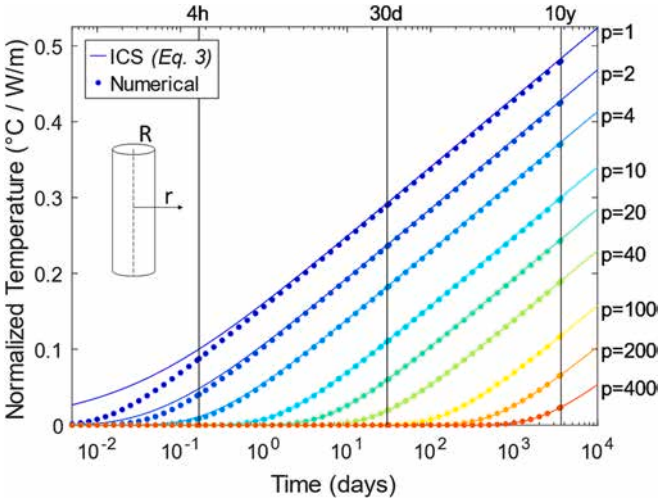

Fig. 2. Comparison between the temperature perturbation normalized by the specific power (q = 100 W/m) given by the ICS method (Ingersoll et al., 1954) (Eq. (5)) and the numerical simulations for only conduction at different distances (p = r/R) with $\lambda = 2$ W/mK and $\alpha = 6.6e\text{-}7$ m^2/s. Three vertical lines highlight 4 h, 30 days and 10 years after the heat injection; $Fo = 3.8$, 690 and $8.4 * 10^4$, respectively, for the thermal parameters in the example.

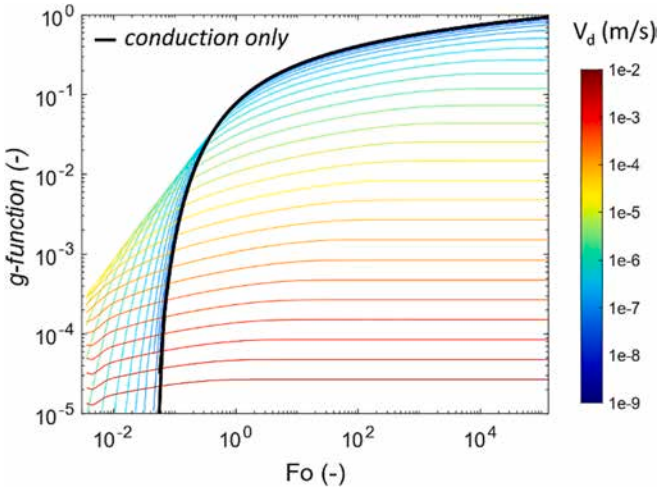

Fig. 3. Numerically derived pseudo g-functions (colored lines) expressed as a function of the Fourier number (Fo) for different Darcy velocities compared to the static groundwater (conduction only) g-function solution obtained with Eq. (6) (black line).

required length of a BHE to satisfy a desired heating power Q_h is obtained by means of the following equation (henceforward only heating will be treated for conciseness, but cooling can be similarly addressed following Kavanaugh and Rafferty (2014)):

$$L_H = \frac{\left(\frac{Q_{Gh}*EFLH_h - Q_{Gc}*EFLH_c}{8760}\right)*\boldsymbol{R_{g3}} + Q_{Gh}*\left(R_b + PLF*\boldsymbol{R_{g2}} + F_{sc}*\boldsymbol{R_{g1}}\right)}{\Delta T} \quad (9)$$

where Q_{Gh} and Q_{Gc} are the heating and cooling loads on the ground, $EFLH_h/EFLH_c$ are the annual equivalent full-load hours for heating and cooling, R_b is the equivalent thermal resistance of the borehole wall and grout, PLF is a term that accounts for the working hours of the day and F_{sc} considers possible thermal short-circuiting due to mutual interactions of BHEs in case of multiple arrangement. Converting the thermal loads on the ground (Q_{Gh} and Q_{Gc}) into thermal loads on the heat pump (building) side ($Q_h = Q_{Gh}*COP/(COP-1)$ and $Q_c = Q_{Gc}*COP/(COP+1)$) by means of the coefficient of performance (COP) and assuming the building design load $Q_h = Q_c$, Eq. (9) can be rewritten to obtain the technical geothermal potential (P_{GSHP}) for a single GSHP with specific configurations:

$$P_{GSHP} = \frac{Q_h}{L} = \frac{\Delta T}{\frac{\frac{COP-1}{COP}EFLH_h - \frac{COP+1}{COP}EFLH_c}{8760}\boldsymbol{R_{g3}} + \frac{COP-1}{COP}\left(R_b + PLF\,\boldsymbol{R_{g2}} + F_{SC}\,\boldsymbol{R_{g1}}\right)} \quad (10)$$

In this study a borehole thermal resistance (R_b) of 0.09 mK/W was used considering a typical double-U configuration (Shonder and Beck, 1999), a PLF of 0.3 and a ΔT of 15 °C were used as common operative values (Kavanaugh and Rafferty, 2014). Furthermore 5 scenarios were compared considering progressively unbalanced conditions from 2400 $EFLH_h$/1600 $EFLH_c$ (energetically balanced considering a COP of 5) to 2400 $EFLH_h$/0 $EFLH_c$ (fully unbalanced scheme, only heating expected).

Ignoring the characteristics of the borehole, the working hours and the operating temperature, the technical potential (P_{GSHP}) can be simplified to obtain a formulation for the theoretical potential (following the definition proposed by Bayer et al. (2019)) that considers only the behavior of the surrounding ground (P_{ground}) at short-/medium-term for an energetically balanced system (i.e., no ground heat storage/extraction occurs after one annual cycle: $q_{Gh}*EFLH_h = q_{Gc}*EFLH_c$)

$$P_{ground} = \frac{1}{\boldsymbol{R_{g2}} + \boldsymbol{R_{g1}}} \quad (11)$$

In other words, Eq. (11) expresses the heat extraction/injection rate the ground is able to ensure by a unit temperature difference ($\Delta T = 1°C\ or\ K$) for a fully operating month (PLF = 1) adding some additional heat extraction/injection in peak conditions (4 h duration pulse).

Eq. (11) assumes that the amount of heat extracted from the ground during heating is compensated during cooling ($E_{Gh} = E_{Gc}$), maintaining the mean annual ground temperature constant and equal to the initial value. If this assumption fails, some heat will be stored/removed in/from the subsurface causing a positive/negative long-term trending thermal perturbation which will affect the ground heat exchange rate. Finally, the ground thermal exchange potential (P_{ground}) for an energetically unbalanced system can be simplified by the following equation:

$$P_{ground} = \frac{1}{(E_{Gh} - E_{Gc})*\boldsymbol{R_{g3}} + \boldsymbol{R_{g2}} + \boldsymbol{R_{g1}}} \quad (12)$$

2.4. A surrogate model to assess the thermal exchange potential at regional scale

The aim of this work was to obtain a comprehensive solution to evaluate and compare the thermal exchange potential of the subsurface covering a wide range of hydrogeological conditions, including the groundwater flow velocity. To this aim, the thermal resistances Rg_1, Rg_2 and Rg_3 were calculated according to Section 2.3 for a total of 5670 combinations of input parameters (V_d, n and S) from the corresponding values of the numerically derived pseudo g-functions in Section 2.2. The relationship between the input variables and the ground thermal resistances was reproduced testing different multi-variate statistical regression (machine learning) models obtaining a surrogate model solution (i.e. the surrogate model returns the response of the underlying 3D FEM model by "picking" its response from a given set of input parameters as defined by the review of Asher et al. (2015)).

After splitting the dataset into training (70 %), validation (15 %) and testing (15 %) subsets, a total of 7 supervised machine learning regression models was tested such as linear regression, support vector machines (SVM), decision trees, Gaussian process regression (GPR) and single layer artificial neural networks (ANN) in Matlab® environment. The best performance in terms of prediction and absence of outliers was obtained by a wide-layer ANN algorithm achieving a R^2 higher than 0.999 and a root mean squared error (RMSE) of 2.0e-3 as shown by Table 4 in comparison with the performance of all the tested models. Note that since all physically realistic parameter combinations are within the modeled range, the surrogate solution can be used to make predictions only within the range of the training parameters.

The parametric study of the thermal response of the ground was reproduced by the selected ANN model, which fully covers the variability of the input parameters, and was used to derive the "theoretical" ground thermal exchange potential (P_{ground}) and the "technical" GSHP thermal exchange potential (P_{GSHP}), by means of Eqs. (10) and (11), respectively, as shown in Fig. 4. The ratio between the heat transported by advection and conduction is also shown by the Peclet number ($Pe = V_d/\alpha$) derived for a value of diffusivity α = 6.6e-7 m^2/s (α ranges between 2.6 * 10^{-7} and 1.3 * 10^{-6} m^2/s for the investigated scenarios).

Due to ground saturation the GSHP thermal potential can rise by 4.8 (n = 0.1) to 7.0 (n = 0.5) times from fully unsaturated to saturated conditions. Due to the material porosity (and the associated thermal parameters) the thermal potential can rise by 1.2 (S = 100) to 1.7 (S = 0) times for porosity from n = 0.5 to n = 0.1, respectively. If groundwater flow is considered, the ground thermal potential can rise by up to two orders of magnitude from static or very low groundwater flow regimes ($Pe < 0.1$) to high values (up to 1e-3 m/s) of Darcy flow velocity ($Pe > 0.1$). This is reflected by an expected increase of the GSHP thermal potential due to groundwater flow up to 3 times. The independence of the results from the total thickness of the model (vertical scalability) was tested comparing three scenarios of thickness (i.e., H = 50, 100 and 200 m) and adjusting the saturation (S) accordingly (note that S is formulated as a percentage of the model total thickness).

Finally, integrating the surrogate model results into a GIS environment, a spatial representation of P_{ground} and P_{GSHP} can be obtained for any groundwater flow regime and mapped over large areas upon the availability of required input data. Note that since the proposed model is valid for a wide range of variability of the input parameters (i.e. flow velocity, porosity and aquifer saturation) and the length-specific response (P_{ground} or P_{GSHP}) is independent from the total thickness of the aquifer, this solution is very flexible and suitable for almost all sedimentary basins around the world considering typical values of groundwater flow regimes and aquifer characteristics (Alley et al., 1999). In this study, a demonstration area in Italy was selected due to

Table 4
Performance of the tested machine learning regression models expressed as the root mean square error (RMSE) and R^2 of the validation (V) and test (T) sets.

Model type	RMSE (V)	RMSE (T)	R^2 (V)	R^2 (T)
ANN	2.0E-03	2.0E-03	1.00	1.00
GPR	1.7E-02	3.5E-03	1.00	1.00
Decision tree	1.1E-01	1.3E-01	0.99	0.99
SVM	1.3E-01	1.3E-01	0.99	0.99
Kernel	1.9E-01	3.9E-01	0.98	0.93
Linear regression	1.2E+00	1.3E+00	0.30	0.13
Stepwise linear regression	1.4E+00	1.3E+00	0.10	0.16

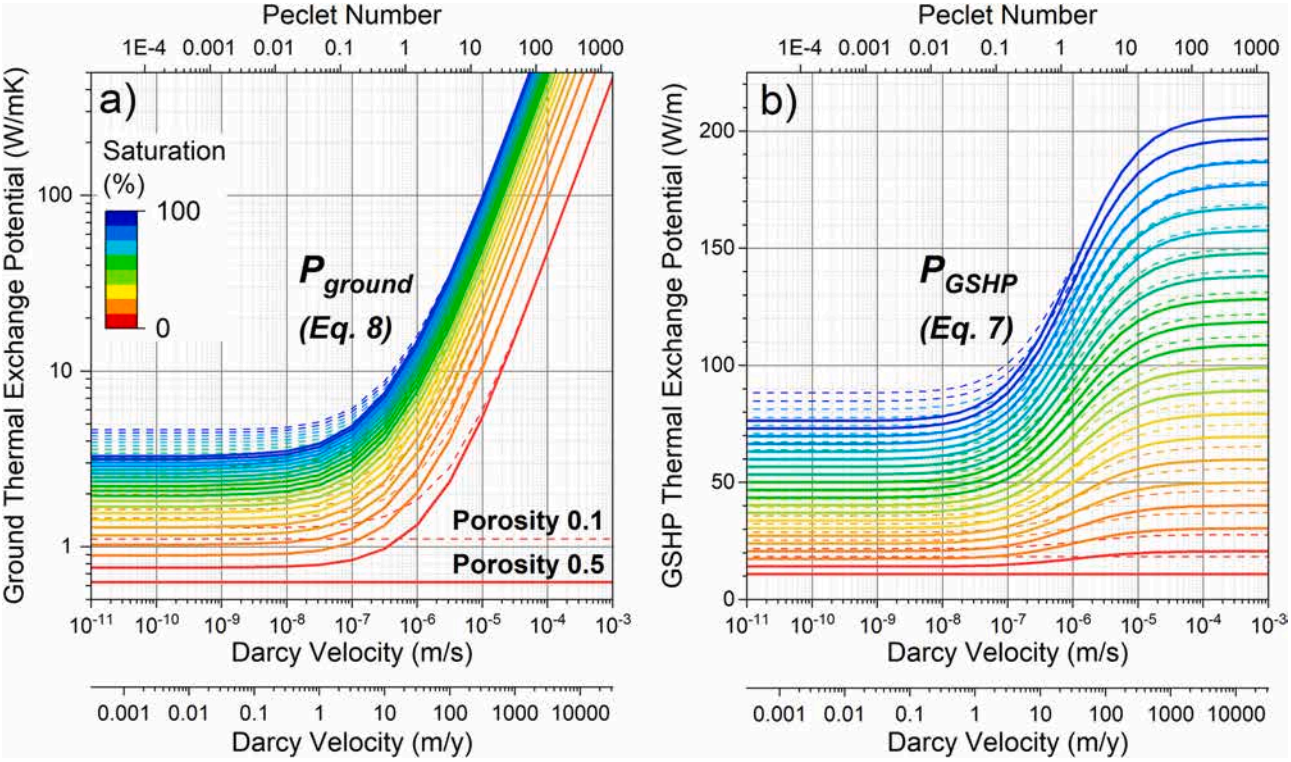

Fig. 4. Modeled thermal exchange potential as a function of the Darcy velocity (V_d), porosity (n) and saturation (S). The left hand plot (a) shows the behavior of the ground (theoretical potential – P_{ground}, Eq. (11)), without considering the BHE thermal resistance and operating temperature, while the right hand plot (b) shows the behavior of the ground + BHE (technical potential – P_{GSHP}, Eq. (10)). The upper axis shows the Peclet number for a value of diffusivity $\alpha = 6.6e\text{-}7\ m^2/s$. Note that the y-axis is logarithmic for (a) and linear for (b).

the high variability of the groundwater flow velocity within the area, so that the corresponding increase in the thermal exchange potential estimated by this model due to advection could be fully illustrated.

3. Study case: the Po plain area, Italy

The demonstration site covers a portion of the alluvial Po plain located in the Lombardia region, northern Italy, for a total area of 12,500 km^2. The proposed methodology is applied over this area showing significantly variable hydrogeological regimes while maintaining the assumptions of the method valid (i.e. this method assesses the thermal exchange potential of the only ground, neglecting the thermal resistance of the borehole, and of the BHE/ground compound system, assuming a constant thermal load applied to a vertical line that can be approximated to the ICS solution by considering the length-to-diameter ratio). Hydrogeological data for this analysis were collected from different datasets and homogenized on a 250 × 250 m grid to serve as inputs for the surrogate model.

3.1. Hydrogeologic setting – input data

The Po Plain area is a peculiar double foreland basin surrounded by two mountain chains (the Alps and the Apennines) representing the feeding sources (Livani et al., 2023). It hosts a sequence of deposits up to 8 km-thick characterized by deep Pliocene to Early Pleistocene marine sediments at the bottom, followed (moving upwards) by the progradation of alluvial deposits during major Quaternary glaciations (Garzanti et al., 2011). To the north, subsurface clastic bodies fed from Alpine rivers are extensive and dominated by coarse deposits, reflecting high detrital supply. To the south, fans fed from Apennine rivers are small, embedded in fine layers reflecting lesser detrital production and abundance of mudrocks in source areas (Ori, 1993). Thanks to intensive geological explorations for oil research and water supply/management purposes, several datasets containing direct and indirect geological and hydrogeological information are available in the study area ([dataset] Regione Lombardia, 2022a).

First, a regional scale groundwater head map available for the year 2014 (shown in the Supplementary materials) was retrieved from the regional environmental database ([dataset] Regione Lombardia, 2022a). From the groundwater head map and the digital elevation model (DEM), the percentage of saturation (S) of the subsurface between 0 and 100 m below the ground level (reference BHE depth for this study) was obtained by:

$$S = 100 - (DEM - Groundwater\ Head) \quad (13)$$

Hydrogeological information were derived collecting and digitalizing 5319 qualitative borehole logs reaching at least −100 m below the ground surface from the regional geological database ([dataset] Regione Lombardia, 2022a). Following the methodology proposed by Previati and Crosta (2021) for a smaller area, the hydrogeological parametrization of the subsurface was done combining the qualitative hydro-facies classification of the borehole stratigraphies with empirical estimations of the porosity and hydraulic conductivity from the analysis of 1467 grain-size distributions. Finally, for each available borehole, equivalent hydraulic parameters for a reference depth of 100 m were computed as the thickness-weighted average of the values assigned to each stratigraphic unit, and interpolated over the study area (the spatial distribution of the equivalent horizontal hydraulic conductivity (K) and porosity (*n*) is provided in the Supplementary material).

Then, the resulting horizontal (depth averaged) Darcy groundwater flow velocity (V_d) was derived combining the equivalent horizontal hydraulic conductivity (K) map with the hydraulic gradient (*i*) map, obtained from the slope of the groundwater head, by means of the Darcy's Law ($V_d = K^*i$). Fig. 5 shows the spatial distribution of two input parameters for the proposed model (the porosity map is shown in the Supplementary materials): the percentage of saturation (S) and the

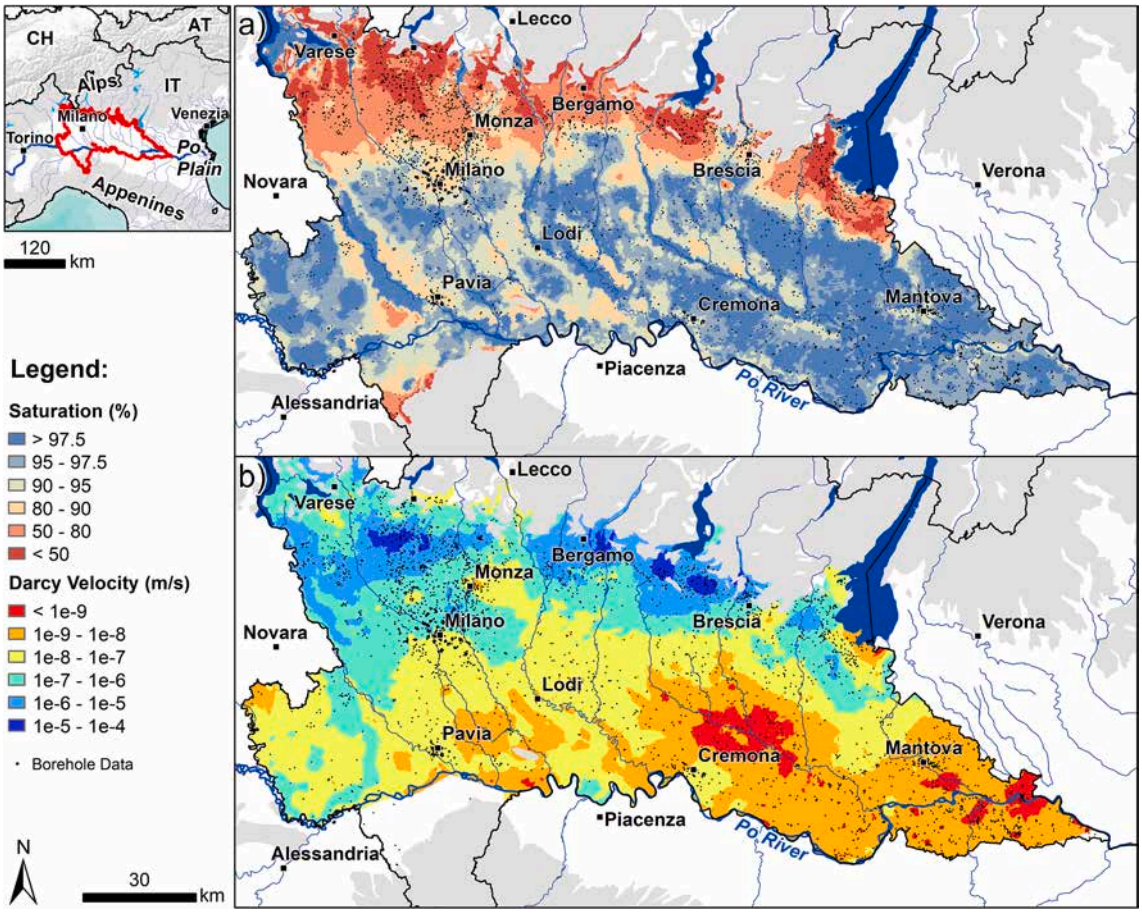

Fig. 5. Maps of the spatial distribution of the percentage of saturation (S) and the equivalent (depth averaged) horizontal Darcy velocity (V_d) of a 100 m thick reference column (extending from the ground surface to a depth of 100 m).

equivalent Darcy flow velocity (V_d) of a 100 m thick reference column (extending from the ground surface to a depth of 100 m).

3.2. Results

The thermal exchange potential was calculated by mean of the surrogate ML model for 318,646 single combinations of input parameters representing the hydrogeologic setting computed for each cell of the analysis grid (cell size is 250 × 250 m). For each combination of input parameters, the ground (P_{ground}) and the GSHP (P_{GSHP}) thermal exchange potentials were calculated both considering only the heat conduction (i.e. assuming $V_d = 0$) and the coupled conductive/advective solution (i.e. considering the estimated groundwater flow velocity). Fig. 6 shows the model results for the demonstrative study area. In particular, it is shown the statistical distribution of the Darcy velocity, the thermal potential considering conduction and advection (both using the solution for the only ground and for the GSHP), and the ratio between the conductive/advective and the conductive solutions as a function of the Darcy velocity. The proposed methodology shows an increase up to 50 times of the ground thermal exchange potential (P_{ground}) due to the heat replenishment caused by advection in areas with a high Darcy flow velocity (i.e. higher than $5 * 10^{-8}$ m/s or 1 m/d) which is reflected by an increase up to 2.3 times of the GSHP thermal exchange potential (P_{GSHP}) considering the characteristics of the geothermal system in this example.

Finally, the spatial distribution of the conductive and the conductive/advective GSHP potentials is shown in Fig. 7. A large increase was observed in the northern sector of the study area where, despite the lower saturation of the shallow aquifer (the depth of the groundwater is between 20 and 50 m from the ground surface, giving S between 80 and 50 %), the GSHP conductive/advective potential was estimated between 80 and >140 W/m compared to values between 50 and 70 W/m if only conduction is considered. On the southern side of the study area, no significant differences were found due to the lower groundwater velocity as shown in Fig. 5.

4. Discussion

4.1. Theoretical and technical thermal potential in advective-dominated regimes

Different solutions have been presented to estimate the thermal exchange potential considering heat conduction around an infinite line source and transport by groundwater flow. A first solution (P_{ground} - Eq. (11)), which considers only the characteristics of the ground (i.e., as if the heat source were a line of infinitesimal thickness without the structure of the BHE), shows the heat extraction/injection rate that the ground is able to ensure by a unit temperature difference ($\Delta T = 1$ °C or K) for a given time. A more complex formulation (P_{GSHP} - Eq. (10)) was then used to derive the thermal exchange potential of a vertical BHE buried in the ground with specific system characteristics such as the equivalent thermal resistance of the borehole, the operating temperature, the operating hours and the COP. This formulation, which still considers the heat exchange properties of the ground and the contribution of moving groundwater, introduces some limitations due to the real geometry and operating profile of a system. According to Bayer et al. (2019), the two solutions can be referred to as the maximum theoretical potential of the ground and the technical potential for a single GSHP configuration.

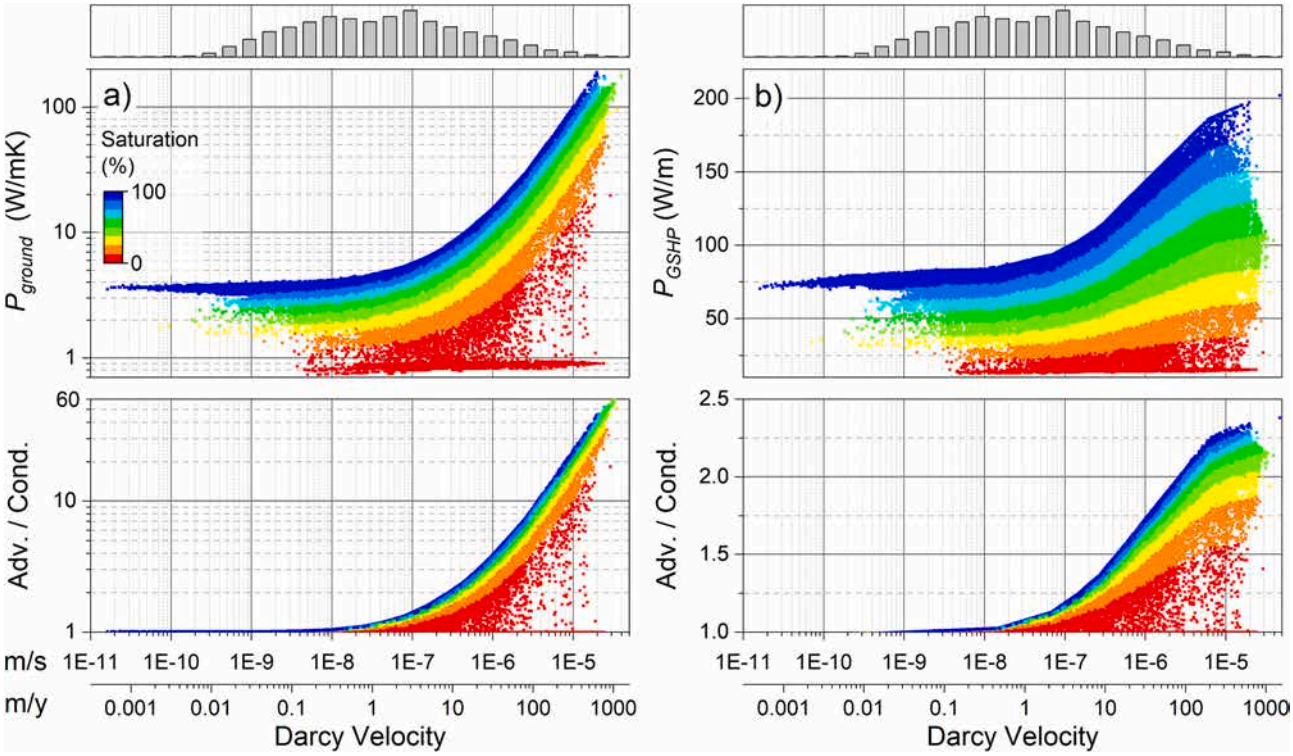

Fig. 6. Comparison between the thermal exchange potential of the ground (a) and the GSHP (b) calculated for all the 318,646 grid cells (250 × 250 m) in the study area and plotted as a function of the Darcy flow velocity. The upper panels show the statistical distribution of the Darcy velocity. The lower plots show the ratio between the advective/conductive solution and the purely conductive (ignoring groundwater flow) solution of the potentials. The points are colored according to the percentage of saturation (S). Note that the y-axis is logarithmic for (a) and linear for (b).

Fig. 8 shows the theoretical (P_{ground} - Eq. (11)) and technical potential (P_{GSHP} - Eq. (10)) for different groundwater flow velocities. For comparison, P_{ground} was multiplied by the same temperature perturbation (ΔT) used for the estimation of P_{GSHP}. The difference between P_{ground} * ΔT (dashed line in Fig. 8) and P_{GSHP} (solid lines in Fig. 8) is named "unusable power" because it shows the additional heat extraction rate the ground could provide, and that cannot be taken by the GSHP system described in this example (which can support only the "usable power"). As we move into regions with strong groundwater flow, the technical potential is higher and, at the same time, the unusable power becomes much larger. This proves that moving groundwater improves the heat exchange with the subsurface, but it could do even more if, for example, the thermal diffusivity of the borehole is designed to maximize heat transfer between the heat source (BHE pipe) and the surrounding ground. Surely this is an area where research should be focused to maximize the efficiency of BHE in high groundwater flow regimes.

4.2. Benefits of the groundwater flow on the long-term potential

The negative effects on the thermal exchange potential of an energetically unbalanced operating scheme depend on the ratio between the energy injected into the ground (E_{Gc}) to the energy extracted (E_{Gh}), and on the long-term ground thermal resistance (R_{g3}). The surrogate model was used to test the performance of a GSHP system under different groundwater flow regimes with progressively energetically unbalanced operating schemes. The reference scenario is a perfectly balanced configuration with 2400 $EFLH_h$ and 1600 $EFLH_c$ considering a COP of 5 ($E_{Gc}/E_{Gc} = 1$). Then the $EFLH_c$ was lowered to 1200, 800, 400 and 0 to obtain different ratios of the energy injected into the ground (E_{Gc}) to the energy extracted (E_{Gh}), from 0.75 to 0. Fig. 9 shows that according to Eq. (10) the thermal potential of an energetically unbalanced system can drop to about 80 % of the corresponding balanced configuration. This difference becomes negligible as the groundwater flow increases, due to the heat replaced by advection which prevents the ground/groundwater temperature to deviate from its initial conditions.

4.3. Comparison with site-specific measurements

Finally, the proposed model was compared with 74 in situ thermal response tests (TRT) data ([dataset] Regione Lombardia, 2022b) available in the study area (see Fig. 7 for their location) for GSHP installations with peak load >50 kW and a mean, min and max depth of 112, 40 and 200 m, respectively. The depth-averaged (up to the BHE bottom) equivalent thermal conductivity (λ) of the ground derived from TRT was compared with the technical potential for GSHP using both the conductive solution and the conductive/advective solution proposed in this study. Despite the poor quality of the field data, a slight correlation was found between the empirical λ and the conductive/advective P_{GSHP} ($R = 0.23$, p-value $= 0.049$), in contrast to what can be observed when compared with the purely conductive P_{GSHP} ($R = -0.06$, p-value $= 0.55$). Fig. 10 shows the statistics of the GSHP thermal potential (in grey the conductive solution, in red the conductive/advective solution) grouped by thermal conductivity classes every 0.5 W/mK. Thus, assuming that there is no significant variation in the mineralogical composition of the deposits in the study area, the equivalent thermal conductivity must, with great caution, be between 1.5 and 3.0 W/mK. Higher values must be related to non-mineralogical influences, such as the studied effects of groundwater flow, as highlighted also by Galgaro et al. (2021) in a comprehensive analysis of TRT data in different geological settings of Italy and by Signorelli et al. (2007) and Wagner et al. (2013) from numerical experiments.

5. Conclusions

The influence of groundwater flow on the thermal exchange potential of ground source heat pumps (GSHP) was quantitatively investigated

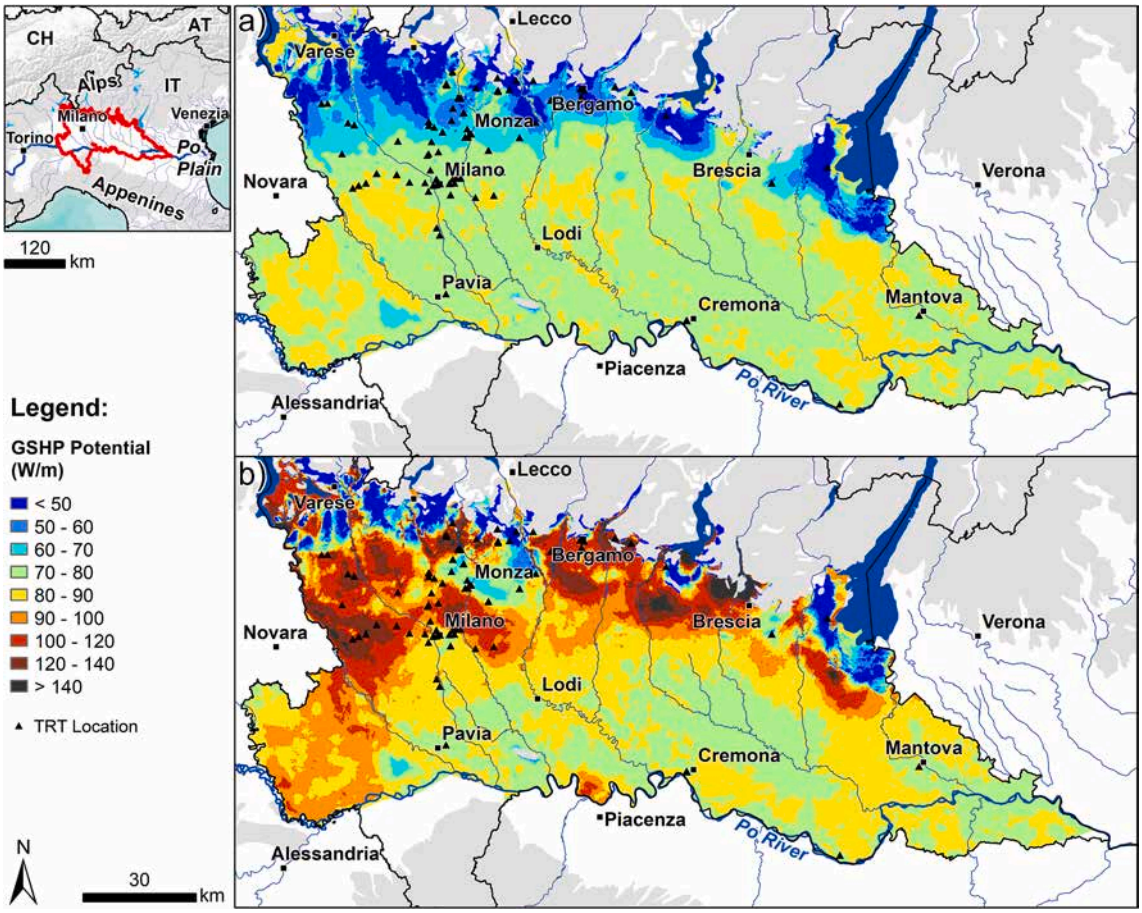

Fig. 7. Maps showing the spatial distribution of the calculated heat exchange potential (P_{GSHP}) with a purely conductive solution (a) and the potential considering the advective heat transport (b). The location of public available thermal response tests (TRT) is shown by black triangles.

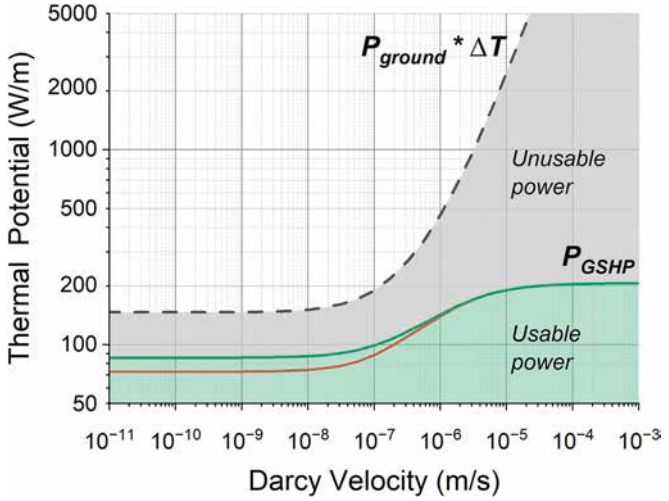

Fig. 8. Comparison between the theoretical thermal potential P_{ground} (dashed line) and the technical potential P_{GSHP} (solid lines) calculated for different groundwater flow velocities. The green line represents the usable power for an energetically balanced operating scheme, whereas the red line represents the case of a fully energetically unbalanced operating scheme. The grey area represents the unusable power due to the characteristics of the BHE and operating scheme.

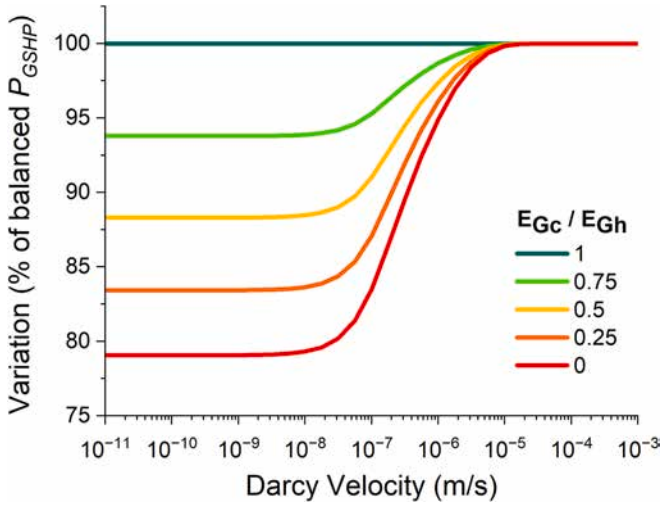

Fig. 9. Comparison between the GSHP thermal potential of a perfectly energetically balanced configuration ($E_{Gc}/E_{Gh} = 1$) and progressively energetically unbalanced operating schemes (e.g., $E_{Gc}/E_{Gh} = 0$ is for heating only).

by means of a synthetic FEM numerical model reproducing the ILS/ICS configuration and covering a wide range of hydrogeological settings. A new solution is proposed to evaluate the thermal resistance of the ground subject to groundwater flow from numerically derived pseudo g-functions under coupled conductive/advective conditions. The proposed model well replicates the existing analytical solutions based on thermal

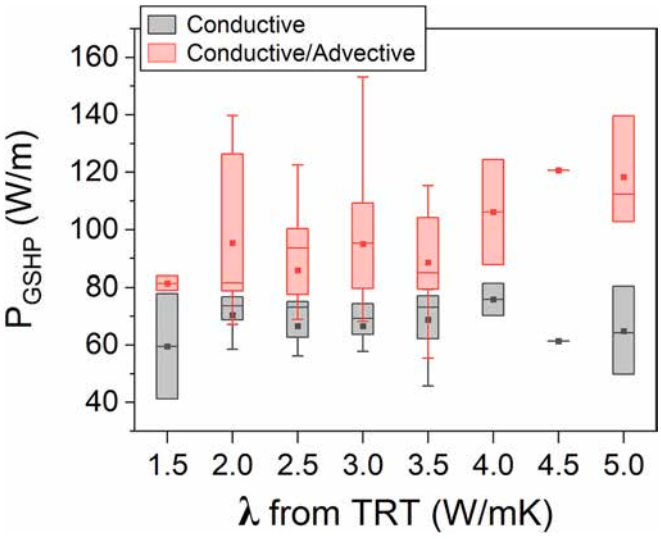

Fig. 10. Comparison between the estimated thermal conductivity (λ) from in situ thermal response tests (TRT) and the calculated thermal potential of GSHP (P_{GSHP}) using the conductive solution (grey boxplots) and the conductive/advective solution (red boxplots) showing a positive correlation only for the conductive/advective solution. Due to the limited number and the poor quality of the field data, the conductivity dataset was grouped into discrete classes every 0.5 W/mK.

diffusion, and goes beyond providing an innovative method for the quantification and regional mapping of the geothermal potential considering the thermal transport by groundwater and the aquifer saturation. The nonlinear response from the synthetic numerical analysis was implemented into a surrogate modeling scheme by fitting the parametric solution with a machine learning regression algorithm. This solution, beyond the run time of the numerical parametric study and the ML training phase, is very fast, applicable at any scale and scalable to any desired depth. Note that since the proposed model is valid for a wide range of variability of the input parameters (i.e., aquifer thickness and saturation, aquifer porosity and groundwater flow velocity) and the length-specific response of the model (i.e., P_{ground} or P_{GSHP}) is independent from the total thickness of the aquifer, this solution is very flexible and suitable for almost all sedimentary basins around the world.

A comparison between the thermal potential calculated considering only heat conduction and the conductive/advective potential showed that for typical groundwater flow regimes the heat extraction rate of a GSHP could be increased up to three times, resulting in a possible significant reduction of the investment costs. If the thermal resistance of the BHE is neglected, the thermal exchange potential of the ground considering the heat replenishment by groundwater advection could be much higher (up to 50 times for a Darcy velocity of 10^{-4} m/s), meaning that in fast moving groundwater environments there is a lot of untapped potential. Research efforts are needed to explore possible engineering solutions to maximize the heat extraction rate in promising areas with strong advection. However, deeper hydrogeologic investigations are also needed to assure the long-term stability of the groundwater flow to minimize the investment risks and avoid undersized systems. Future perspectives may include an empirical validation of the proposed method at the BHE scale, testing the performance under artificially induced advective regimes and the implementation of the conductive/advective pseudo g-functions for multiple borehole arrays. This approach could also be implemented introducing heterogeneous groundwater flow velocities along the vertical direction.

Thanks to the developed surrogate model, the conductive/advective thermal exchange potential of the ground only (P_{ground}) and of a vertical GSHP buried in the ground (P_{GSHP}) was evaluated over a demonstrative large area in northern Italy, showing a great variability due to the groundwater flow regime governed by the permeability of the deposits and the natural hydraulic gradient between the Alpine foothills and the center of the Po alluvial plain. Promising results were obtained in locations close to reliefs where the groundwater flow is higher and energy demand is high, paving the way for direct tests to validate these results in similar areas worldwide. Therefore, the proposed model aims to be a regional scale quantitative management tool applicable in any geological setting composed of loose deposits, for any hydrogeological regime and for any GSHP configuration, with strong implications for planning the development of shallow geothermal applications around the world.

CRediT authorship contribution statement

Alberto Previati: Visualization, Software, Methodology, Data curation, Conceptualization, Writing – review & editing, Writing – original draft. **Giovanni Crosta:** Supervision, Conceptualization, Writing – review & editing.

Declaration of competing interest

The authors declare that they have no known competing financial interests or personal relationships that could have appeared to influence the work reported in this paper.

Data availability

Data sources are reported in the references as [datasets]

Acknowledgments

This article is an outcome of the research agreement between University of Milano-Bicocca (DISAT) and Gruppo CAP: "Analisi del potenziale geotermico alla scala di bacino idrico gestito da Gruppo CAP" and of the PRIN Project 2017HPJLPW “URGENT – Urban geology and geohazards: Engineering geology for safer, resilient and smart cities” funded by MIUR.

Appendix A. Supplementary data

Supplementary data to this article can be found online at https://doi.org/10.1016/j.scitotenv.2023.169046.

References

Alcaraz, M., García-Gil, A., Vázquez-Suñé, E., Velasco, V., 2016. Advection and dispersion heat transport mechanisms in the quantification of shallow geothermal resources and associated environmental impacts. Sci. Total Environ. 543, 536–546. https://doi.org/10.1016/j.scitotenv.2015.11.022.

Alley, W.M., Reilly, T.E., Franke, O.L., 1999. Sustainability of Ground-Water Resources. US Department of the Interior, US Geological Survey.

Angelotti, A., Alberti, L., La Licata, I., Antelmi, M., 2014. Energy performance and thermal impact of a Borehole Heat Exchanger in a sandy aquifer: influence of the groundwater velocity. Energy Convers. Manag. 77, 700–708. https://doi.org/10.1016/j.enconman.2013.10.018.

Asher, M.J., Croke, B.F.W., Jakeman, A.J., Peeters, L.J.M., 2015. A review of surrogate models and their application to groundwater modeling. Water Resour. Res. 51, 5957–5973. https://doi.org/10.1002/2015WR016967.

Banks, D., 2015. A review of the importance of regional groundwater advection for ground heat exchange. Environ. Earth Sci. 73, 2555–2565. https://doi.org/10.1007/s12665-014-3377-4.

Bayer, P., Attard, G., Blum, P., Menberg, K., 2019. The geothermal potential of cities. Renew. Sust. Energ. Rev. 106, 17–30. https://doi.org/10.1016/J.RSER.2019.02.019.

BLOCON, 2015. Earth energy designer (EED) version 3.2. https://buildingphysics.com/eed-2/.

Böttcher, F., Casasso, A., Götzl, G., Zosseder, K., 2019. TAP - thermal aquifer potential: a quantitative method to assess the spatial potential for the thermal use of groundwater. Renew. Energy 142, 85–95. https://doi.org/10.1016/j.renene.2019.04.086.

Carslaw, H.S., Jaeger, J.C., 1959. Conduction of Heat in Solids, 2nd ed. Clarendon Press, Oxford.

Casasso, A., Sethi, R., 2016. G.POT: a quantitative method for the assessment and mapping of the shallow geothermal potential. Energy 106, 765–773. https://doi.org/10.1016/j.energy.2016.03.091.
Casasso, A., Sethi, R., 2017. Assessment and mapping of the shallow geothermal potential in the province of Cuneo (Piedmont, NW Italy). Renew. Energy 102, 306–315. https://doi.org/10.1016/j.renene.2016.10.045.
Casasso, A., Pestotnik, S., Rajver, D., Jež, J., Prestor, J., Sethi, R., 2017. Assessment and mapping of the closed-loop shallow geothermal potential in Cerkno (Slovenia). Energy Procedia 125, 335–344. https://doi.org/10.1016/j.egypro.2017.08.210.
Choi, J.C., Park, J., Lee, S.R., 2013. Numerical evaluation of the effects of groundwater flow on borehole heat exchanger arrays. Renew. Energy 52, 230–240. https://doi.org/10.1016/j.renene.2012.10.028.
Diao, N., Li, Q., Fang, Z., 2004. Heat transfer in ground heat exchangers with groundwater advection. Int. J. Therm. Sci. 43, 1203–1211. https://doi.org/10.1016/j.ijthermalsci.2004.04.009.
Domenico, P.A., Schwartz, F.W., 1998. Physical and Chemical Hydrogeology. Wiley.
Eskilson, P., 1987. Thermal Analysis of Heat Extraction Boreholes. Sweden.
Fan, R., Jiang, Y., Yao, Y., Shiming, D., Ma, Z., 2007. A study on the performance of a geothermal heat exchanger under coupled heat conduction and groundwater advection. Energy 32, 2199–2209. https://doi.org/10.1016/j.energy.2007.05.001.
Fienen, M.N., Nolan, B.T., Feinstein, D.T., Starn, J.J., 2015. Metamodels to bridge the gap between modeling and decision support. Groundwater 53, 511–512. https://doi.org/10.1111/gwat.12339.
Fienen, M.N., Nolan, B.T., Feinstein, D.T., 2016. Evaluating the sources of water to wells: three techniques for metamodeling of a groundwater flow model. Environ. Model. Softw. 77, 95–107. https://doi.org/10.1016/j.envsoft.2015.11.023.
Fujii, H., Itoi, R., Fujii, J., Uchida, Y., 2005. Optimizing the design of large-scale ground-coupled heat pump systems using groundwater and heat transport modeling. Geothermics 34, 347–364. https://doi.org/10.1016/j.geothermics.2005.04.001.
Galgaro, A., Di Sipio, E., Teza, G., Destro, E., De Carli, M., Chiesa, S., Zarrella, A., Emmi, G., Manzella, A., 2015. Empirical modeling of maps of geo-exchange potential for shallow geothermal energy at regional scale. Geothermics 57, 173–184. https://doi.org/10.1016/j.geothermics.2015.06.017.
Galgaro, A., Dalla Santa, G., Zarrella, A., 2021. First Italian TRT database and significance of the geological setting evaluation in borehole heat exchanger sizing. Geothermics 94, 102098. https://doi.org/10.1016/j.geothermics.2021.102098.
García-Gil, A., Vázquez-Suñe, E., Alcaraz, M.M., Juan, A.S., Sánchez-Navarro, J.Á., Montlleó, M., Rodríguez, G., Lao, J., 2015. GIS-supported mapping of low-temperature geothermal potential taking groundwater flow into account. Renew. Energy 77, 268–278. https://doi.org/10.1016/j.renene.2014.11.096.
Garzanti, E., Vezzoli, G., Andò, S., 2011. Paleogeographic and paleodrainage changes during Pleistocene glaciations (Po Plain, northern Italy). Earth Sci. Rev. 105, 25–48.
Hecht-Méndez, J., Molina-Giraldo, N., Blum, P., Bayer, P., 2010. Evaluating MT3DMS for heat transport simulation of closed geothermal systems. Ground Water 48, 741–756. https://doi.org/10.1111/j.1745-6584.2010.00678.x.
Ingersoll, L.R., Zobel, O.J., Ingersoll, A.C., 1954. Heat Conduction with Engineering, Geological and Other Applications.
Kavanaugh, S.P., Rafferty, K., 2014. Geothermal Heating and Cooling: Design of Ground-Source Heat Pump Systems (ASHRAE).
Livani, M., Petracchini, L., Benetatos, C., Marzano, F., Billi, A., Carminati, E., Doglioni, C., Petricca, P., Maffucci, R., Codegone, G., Rocca, V., Verga, F., Antoncecchi, I., Torino, P., Università, S., 2023. Subsurface Geological and Geophysical Data From the Po Plain and the Northern Adriatic Sea (North Italy). Earth Syst. Sci. Data Discuss 1–41. https://doi.org/10.5194/essd-2023-65.
Ori, G.G., 1993. Continental depositional systems of the Quaternary of the Po Plain (northern Italy). Sediment. Geol. 83 (1–2), 1–14.
Piga, B., Casasso, A., 2017. Thermal Impact Assessment of Groundwater Heat Pumps (GWHPs): Rigorous Vs. Simplified Models. https://doi.org/10.3390/en10091385.
Previati, A., Crosta, G.B., 2021. Regional-scale assessment of the thermal potential in a shallow alluvial aquifer system in the Po plain (northern Italy). Geothermics 90, 101999. https://doi.org/10.1016/j.geothermics.2020.101999.
Regione Lombardia, 2022a. Regional database of environmental/geological spatial data (Geoportale) [WWW Document]. URL. www.geoportale.regione.lombardia.it/.
Regione Lombardia, 2022b. Regional databse of GSHP installations (Registro Sonde Geotermiche - RGS) [WWW Document]. URL. https://www.dati.lombardia.it/Energia/Elenco-Registro-Regionale-Sonde-Geotermiche/cm2i-qe47.
Shonder, J.A., Beck, J.V., 1999. Field test of a new method for determining soil formation thermal conductivity and borehole resistance. ASHRAE Trans. 106 (1999).
SIA 384/6, 2010. Schweizerischer Ingenieur- und Architektenverein, 2010. In: Erdwärmesonden (Swiss Guidelines for the Installation of Borehole Heat Exchangers).
Signorelli, S., Bassetti, S., Pahud, D., Kohl, T., 2007. Numerical evaluation of thermal response tests. Geothermics 36, 141–166. https://doi.org/10.1016/j.geothermics.2006.10.006.
Spitler, J.D., 2000. GLHEPRO: A Design Tool for Commercial Building Ground Loop Heat Exchangers.
Spitler, J.D., Bernier, M., 2016. Vertical borehole ground heat exchanger design methods. In: Advances in Ground-Source Heat Pump Systems. Elsevier Inc., pp. 29–61. https://doi.org/10.1016/B978-0-08-100311-4.00002-9
Sutton, M.G., Nutter, D.W., Couvillion, R.J., 2003. A ground resistance for vertical bore heat exchangers with groundwater flow. J. Energy Resour. Technol. Trans. ASME 125, 183–189. https://doi.org/10.1115/1.1591203.
VDI 4640/2, 2001. Thermal Use of the Underground — Ground Source Heat Pump Systems (German Guidelines).
Viesi, D., Galgaro, A., Visintainer, P., Crema, L., 2018. GIS-supported evaluation and mapping of the geo-exchange potential for vertical closed-loop systems in an Alpine valley, the case study of Adige Valley (Italy). Geothermics 71, 70–87. https://doi.org/10.1016/j.geothermics.2017.08.008.
Wagner, V., Blum, P., Kübert, M., Bayer, P., 2013. Analytical approach to groundwater-influenced thermal response tests of grouted borehole heat exchangers. Geothermics 46, 22–31. https://doi.org/10.1016/j.geothermics.2012.10.005.
Wang, H., Qi, C., Du, H., Gu, J., 2009. Thermal performance of borehole heat exchanger under groundwater flow: a case study from Baoding. Energy Build. 41, 1368–1373. https://doi.org/10.1016/j.enbuild.2009.08.001.
Woodside, W., Messmer, J.H., 1961. Thermal conductivity of porous media I. Unconsolidated sands. J. Appl. Phys. 32 https://doi.org/10.1063/1.1728419.